

# Journal of Biomedical Optics

[SPIDigitalLibrary.org/jbo](http://SPIDigitalLibrary.org/jbo)

## **Quantitative estimation of mechanical and optical properties from ultrasound assisted optical tomography data**

Mayanglambam Suheshkumar Singh  
Kanhirodan Rajan  
Ram Mohan Vasu  
Debasish Roy

# Quantitative estimation of mechanical and optical properties from ultrasound assisted optical tomography data

Mayanglambam Suheshkumar Singh,<sup>a</sup> Kanhirodan Rajan,<sup>a</sup> Ram Mohan Vasu,<sup>b</sup> and Debasish Roy<sup>c</sup>

<sup>a</sup>Indian Institute of Science, Department of Physics, Bangalore 560012, India

<sup>b</sup>Indian Institute of Science, Department of Instrumentation and Applied Physics, Bangalore 560012, India

<sup>c</sup>Indian Institute of Science, Department of Civil Engineering, Bangalore 560012, India

**Abstract.** We demonstrate quantitative optical property and elastic property imaging from ultrasound assisted optical tomography data. The measurements, which are modulation depth  $M$  and phase  $\phi$  of the speckle pattern, are shown to be sensitively dependent on these properties of the object in the insonified focal region of the ultrasound (US) transducer. We demonstrate that Young's modulus ( $E$ ) can be recovered from the resonance observed in  $M$  versus  $\omega$  (the US frequency) plots and optical absorption ( $\mu_a$ ) and scattering ( $\mu_s$ ) coefficients from the measured differential phase changes. All experimental observations are verified also using Monte Carlo simulations. © 2012 Society of Photo-Optical Instrumentation Engineers (SPIE). [DOI: 10.1117/1.JBO.17.10.101507]

Keywords: absorption coefficient; scattering coefficient; synchronized speckle detection; ultrasound assisted optical tomography.

Paper 11681SS received Nov. 22, 2011; revised manuscript received Mar. 30, 2012; accepted for publication Apr. 18, 2012; published online Jun. 22, 2012.

## 1 Introduction

Soft-tissue organ imaging with near infrared (NIR) light is pursued vigorously because of its application in early diagnosis of cancer based on the measured spectral variation of  $\mu_a$ . This modality known as diffuse optical tomography (DOT) however produces only low resolution images limited by the diffusion propagation of photons through soft tissue with large  $\mu_s$ 's (reduced scattering coefficient). Ultrasound assisted optical tomography (UAOT) is developed as a possible remedy to this poor resolution, which takes advantage of tight focusing of ultrasound (US) waves in tissues and restricting imaging of optical as well as mechanical properties to the focal volume (the region of interest, ROI) using the so-called US-tagged photons. UAOT began by constructing qualitative images of  $\mu_a$  in the ROI from the measured  $M$  of light autocorrelation  $G_1(\tau)$ . There were several attempts to move onto quantitative  $\mu_a$  and  $\mu_s$  recovery<sup>1-4</sup> which began with modeling of US-induced effects in the ROI which are oscillation of scattering centers and refraction index modulation ( $\Delta n$ ).<sup>5-7</sup> Theoretical expressions are derived for  $M$  in terms of the phase modulation ( $\phi$ ) and its fluctuation ( $\Delta\phi$ ) picked-up by light from the ROI which connected  $M$  to  $\mu_a$ ,  $\mu_s$  and also to  $E$ . In spite of the above there were no attempts of quantitative recovery of these properties from  $M$ . This work is intended to primarily fill this gap by quantitative recovery of  $\mu_a$ ,  $\mu_s$  from  $\langle\Delta\phi\rangle$  and  $E$  from  $M$ .  $\Delta\phi$ , as demonstrated here, has a non-zero mean  $\langle\Delta\phi\rangle$  when the US frequency ( $\omega$ ) is small ( $< \text{kHz}$ ) and the anisotropy factor  $g$  is large. The ultrasound modulation can be decreased when the optical scattering increases, thereby reducing the modulation depth of UAOT signals.<sup>3</sup>

Both  $M$  and  $\langle\Delta\phi\rangle$  can be theoretically computed from  $G_1(\tau)$  the amplitude autocorrelation of detected photons arrived at

using the expressions given in Refs. 8 and 9, also Monte Carlo simulation of detected scattered photons. As demonstrated earlier<sup>9</sup>  $\langle\Delta\phi\rangle$  computed using MC simulations is shown to be non-zero for the phantom with large  $g$  (here  $g = 0.89$ ) when  $\omega < 1$  kHz and the insonified volume ( $V_{\text{in}}$ ) does not exceed 3 to 4 times  $(\ell^*)^3$  ( $\ell^*$  is the transport mean path given by  $1/\mu_s'$ ). In this work, because we use  $\langle\phi\rangle$  to compute  $\mu_a$  and  $\mu_s$  changes we would like to keep  $\langle\phi\rangle$  large so that with  $\mu_a$  and  $\mu_s$  there is a large range of variation in  $\langle\phi\rangle$ . For this we keep in our simulations and experiments  $V_{\text{in}} \approx (\ell^*)^3$ . With reference to Fig. 1 the phase fluctuation ( $\Delta\phi$ ) picked up by light in a typical scattering event owing to a displacement of the scatterer by  $\mathbf{u}$  is  $\mathbf{u} \cdot (\hat{k}_s - \hat{k}_i) = |\mathbf{u}| |\hat{k}_s - \hat{k}_i| \cos \frac{\theta}{2}$ . Therefore decorrelation in  $\Delta\phi$  will be dictated by  $\langle\cos \frac{\theta}{2}\rangle$  (and not by  $\langle\cos \theta\rangle$ ) and therefore the anisotropy factor, when considering this decorrelation, should be replaced by  $g_n = \langle\cos \frac{\theta}{2}\rangle$  and  $\ell^*$  used above is arrived from this new  $g_n$  (denoted it by  $\ell_n^*$ ) which is larger than the usual  $\ell^*$ .

First we verify that  $\langle\phi\rangle$  indeed can be non-zero. Theoretically we arrive at a distribution of  $\phi$  at an array of detector points on one face of a slab of dimension  $40 \times 40 \times 50$  mm<sup>3</sup> and optical properties,  $g = 0.89$ ,  $\mu_s = 20$  cm<sup>-1</sup>, and  $\mu_a = 0.18$  cm<sup>-1</sup> by launching ten million photons from a point on the opposite side.<sup>9</sup> From the random distribution of  $\phi$  a histogram of its distribution is computed. It is seen that when  $\omega = 1$  MHz the distribution is uniform with zero mean and when  $\omega = 100$  Hz it has a mean of 130 deg. The figure is not included for want of space. The insonified region for the computation is taken as a cube of volume  $4 \times 7 \times 4$  mm<sup>3</sup> which is  $\sim (\ell_n^*)^3$ . The histogram arrived at from the experimentally measured  $\phi$  is shown in Fig. 2(a) and 2(b) which also verifies almost the same non-zero  $\langle\phi\rangle$  obtained from computation (the experiments are described further down).

Address all correspondence to: Kanhirodan Rajan, Indian Institute of Science, Department of Physics, Bangalore 560012, India. Tel: +91802293280; Fax: +918023602602; E-mail: rajan@physics.iisc.ernet.in

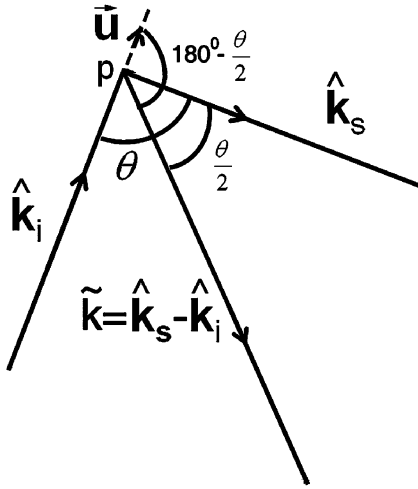


**Fig. 1** A schematic diagram of scattering of light by a scattering center which undergoes vibration with an amplitude  $\mathbf{u}$ . The incident light with wave vector,  $\mathbf{k}_i$  is scattered with an associated wavelength along  $\mathbf{k}_s$ .

We use the histogram to compute  $\langle \phi \rangle$ . To compute  $M$ ,  $G_1(\tau)$  is computed from the arrived photons at a detector which is photon-path probability density weighted (only those paths which intersect ROI are considered) and its Fourier transform amplitudes at  $\omega = \omega_o$  the acoustic frequency is computed. The details are in Ref. 10. The computed as well as experimentally measured  $M$  and  $\langle \phi \rangle$  are used to recover the average  $\mu_a$ ,  $\mu_s$  and  $E$  ( $\langle \mu_a \rangle$ ,  $\langle \mu_s \rangle$  and  $\langle E \rangle$ , respectively) of the insonified ROI in the object, as detailed below.

We calibrate our measurements with respect to  $\mu_a$ ,  $\mu_s$  (against  $\langle \phi \rangle$ ) and  $E$  (against  $M$ ). Theoretically, to get plots of  $M$  versus  $E$  one has to go through a number of steps for a given  $E$ : 1. compute the US radiation force in the ROI, 2. set-up and solve the force-balance equation to find  $\mathbf{u}(\mathbf{r})$  the distribution of US-induced displacement of the scatterers, and 3. transport photons using MC simulation and arrive at  $G_1(\tau)$  and  $M$ . Details of the above steps are given in Ref. 10. While doing the above we can also compute the distribution of  $\phi$  and  $\langle \phi \rangle$ . However, in regard to  $\phi$  we have an easier route which employs the semi-empirical relation first proposed in Ref. 11 in the context of frequency-modulation diffuse optical tomography (DOT) connecting  $\langle \phi \rangle$  and  $\mu_a$ ,  $\mu_s$ , and  $g$ . It is given by

$$\langle \Delta \phi \rangle = \frac{\sqrt{3}d}{\lambda} \sqrt{\frac{\mu_s(1-g)}{\mu_a}}. \quad (1)$$

Here  $d$  is the geometrical distance between sensor and detector,  $\lambda$  is the wavelength of light used, and  $\phi$  has to be interpreted as the phase associated with the intensity modulated photon flux. This has been also shown to be true in UAOT in Ref. 8 with assumption that  $\phi$  is the phase of the mixed low frequency oscillation at the US frequency. In UAOT one computes a differential phase which is

$$\langle \Delta \phi \rangle = \frac{\langle \phi \rangle_o}{\langle \phi \rangle_r}, \quad (2)$$

where  $\langle \phi \rangle_o$  and  $\langle \phi \rangle_r$  are the measured averages corresponding to an inhomogeneity in the ROI and reference homogeneous medium, respectively. It is easily seen that when the local  $\mu_a$  changes from the background  $\mu_a^b$  to  $\mu_a^{\text{in}}$

$$\langle \Delta \phi \rangle_{\mu_a} = \sqrt{\frac{\mu_a^b}{\mu_a^{\text{in}}}}. \quad (3)$$

The corresponding  $\langle \Delta \phi \rangle_{\mu_s}$  when  $\mu_s$  changes is

$$\langle \Delta \phi \rangle_{\mu_s} = \sqrt{\frac{\mu_s^{\text{in}}}{\mu_s^b}}. \quad (4)$$

Equation (1) is verified using data from MC simulation and found to be fairly close representation of the actual variation of  $\langle \phi \rangle$ . The results are not given for want of space.

For extracting  $E$  from  $M$  we made use of the frequency at which a dominant natural mode of vibration of the ROI coincides with the US frequency. The resonance for a jelly like soft tissue mimicking object is at low frequencies and therefore to insonify the object at low frequencies we mix two US beams oscillating at slightly different (and adjustable) frequencies. The mixed difference frequency pressure wave drives the scattering centers in the ROI. The resonance can be observed in the  $M$  versus  $\omega$  plot as a peak, which is first obtained from computed  $M$  and the experiments. At these low frequencies, as observed in Ref. 8, one of the effects of US forcing, namely  $\Delta n$  is small. Therefore, in this study, we neglected  $\Delta n$ . The resonance

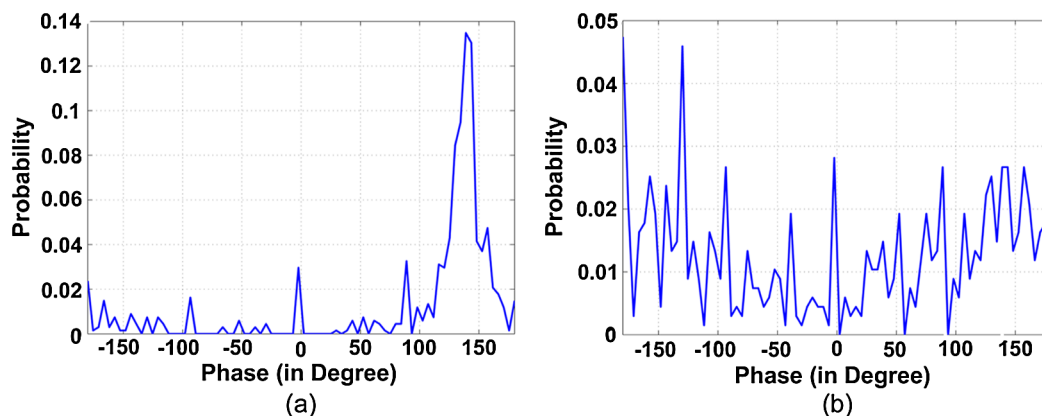


**Fig. 2** (a) Experimental plot of histogram of  $\Delta \phi$  at US beat frequency of 100 Hz. (b) Experimental plot of histogram of  $\Delta \phi$  at US frequency of 1 MHz.



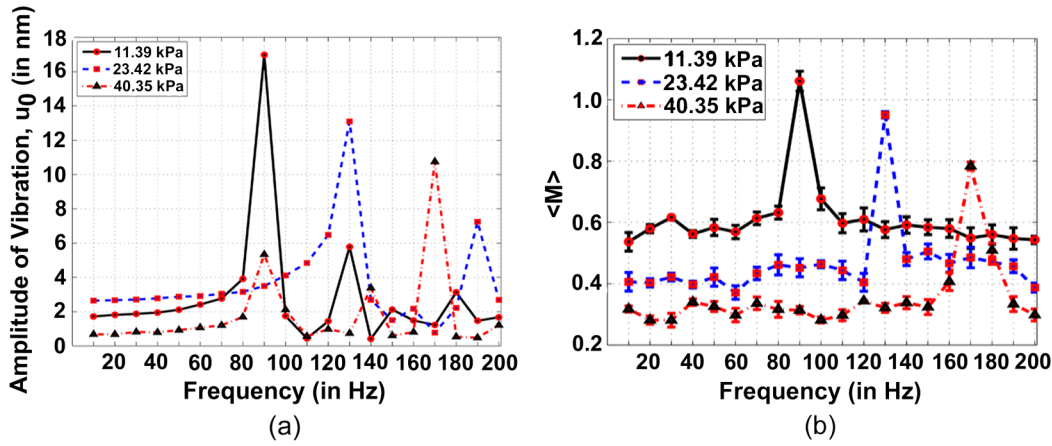


**Fig. 4** (a) The plot of frequency response (amplitude of vibration) of the insonified region against the ultrasound beat frequency using ANSYS package. The elasticity co-efficients used are 11.39, 23.42, and 40.35 kPa. Poisson's ratio of 0.499 and mass density of  $1000 \text{ kg/m}^3$  are used in all the simulations. (b) The experimental plot of the modulation depth ( $M$ ) against the ultrasound beat frequency. The experimental error is in the range 0.46% to 7.80%. PVA phantoms with two, three, and four freeze-thaw cycles which correspond to the elastic co-efficients of 11.39, 23.42, and 40.35 kPa are used.

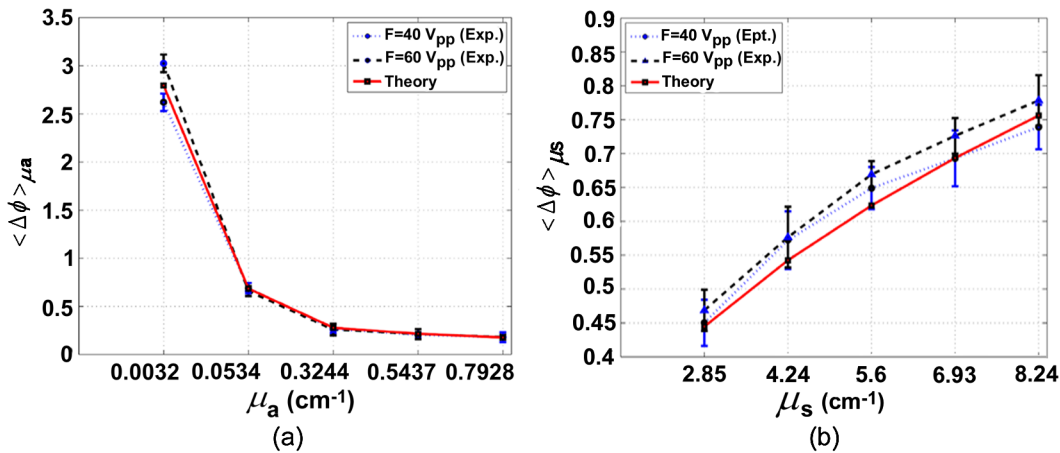


**Fig. 5** The plot of phase =  $\langle \Delta\phi \rangle_o / \langle \Delta\phi \rangle_r$  against (a) absorption coefficient  $\mu_a$  and (b) scattering coefficient  $\mu_s$ . In these plots ultrasound driving voltage is used as experimental parameter with  $40V_{pp}$  and  $60V_{pp}$ . The operating ultrasound modulation beat frequency is 750 Hz. The experimental error is 0.10% to 13.82%. Liquid phantoms are used as the tissue-samples.

$\langle \Delta\phi \rangle_{\mu_s}$ 's are plotted in Fig. 5 which also verify the variation predicted by Eq. (4) leading to a simple read-out of  $\mu_s^{\text{in}}$  from the measured  $\langle \Delta\phi \rangle_{\mu_s}$ .

### 3 Conclusion

In conclusion we have demonstrated the possibility of recovering the average  $\mu_a$ ,  $\mu_s$ , and  $E$  corresponding to the insonified ROI from the UAOT measurements of  $M$  and  $\langle \phi \rangle$ . The hitherto neglected  $\phi$  considering it as a zero-mean random variable is shown to have a non-zero mean when there is a large scattering anisotropy and acoustic frequency is small. This means that  $\langle \phi \rangle$  which carries useful information can be employed for the recovery of optical properties.

The other two advantages of the present study are: 1. Since we have not used a diffusion model in our inversion, the method should work well when the ROI is in a low scattering region like water-filled cyst. 2. Since we concentrate on the ROI, the reconstruction from these are not effected by bulk movement of body (like coming through respiration).

### References

1. C. Kim and L. V. Wang, "Multi-optical-wavelength ultrasound-modulated optical tomography," *Opt. Lett.* **32**(16), 2285–2287 (2007).
2. Y. H. Zhang et al., "Photorefractive detection of tissue optical and mechanical properties by ultrasound modulated optical tomography," *Opt. Lett.* **32**(6), 656–658 (2007).
3. S. R. Kothapalli et al., "Imaging optically scattering objects with ultrasound-modulated optical tomography," *Opt. Lett.* **32**(16), 2351–2353 (2007).
4. A. Brattchenia et al., "Millimeter-resolution acousto-optic quantitative imaging in a tissue model system," *J. Biomed. Opt.* **14**(3), 034031 (2009).
5. L. H. V. Wang, "Mechanisms of ultrasonic modulation of multiply scattered coherent light: an analytical model," *Phys. Rev. Lett.* **87**(4), 043903 (2001).
6. S. Sakadžić and L. V. Wang, "Ultrasonic modulation of multiplyscattered coherent light: an analytical model for anisotropically scattering media," *Phys. Rev. E* **66**(2), 026603 (2002).
7. L. H. V. Wang, "Mechanisms of ultrasonic modulation of multiply scattered coherent light: a Monte Carlo model," *Opt. Lett.* **26**(15), 1191–1193 (2001).

8. M. Suheshkumar Singh et al., "Assessment of ultrasound modulation of near infrared light on the quantification of scattering coefficient," *Med. Phys.* **37**(7), 3744–3751 (2010).
9. M. Suheshkumar Singh et al., "Ultrasound assisted optical tomography: estimation of phase shift experienced by photon on transit through US insonified region for detection of breast tumor," *Proc. SPIE*. **8320**, 832015 (2012).
10. R. S. Chandran et al., "Ultrasound modulated optical tomography: Young's modulus of insonified region from measurement of natural frequency of vibration," *Opt. Exp.* **19**(23) 22837–22850 (2011).
11. B. C. Wilson et al., "Time-dependent optical spectroscopy and imaging for biomedical applications," *Proc. IEEE* **80**(6), 918–930 (1992).
12. ANSYS Rel. 10.0, ANSYS. Inc.